The Kinematic Structure of a Hurricane with Sea Level Pressure Less Than 900 mb

PETER DODGE, ROBERT W. BURPEE,* AND FRANK D. MARKS JR.

Hurricane Research Division, AOML/NOAA, Miami, Florida

(Manuscript received 7 January 1998, in final form 18 June 1998)

ABSTRACT

A National Oceanic and Atmospheric Administration aircraft recorded the first Doppler radar data in a tropical cyclone with a minimum sea level pressure (MSLP) <900 mb during a reconnaissance mission in Hurricane Gilbert on 14 September 1988, when its MSLP was ~895 mb. A previous mission had found an MSLP of 888 mb, making Gilbert the most intense tropical cyclone yet observed in the Atlantic basin.

Radar reflectivity identified the hurricane eye, inner and outer eyewalls, a stratiform region between the eyewalls, and an area outside the outer eyewall that contained a few rainbands but that had mostly stratiform rain. Pseudo–dual Doppler analyses depict the three-dimensional kinematic structure of the inner eyewall and a portion of the outer eyewall. The vertical profiles of tangential wind and reflectivity maxima in the inner eyewall are more erect than in weaker storms, and winds >50 m s^{-1} extended to 12 km, higher than has been reported in previous hurricanes. The inner eyewall contained weak inflow throughout most of its depth. In contrast, the portion of the outer eyewall described here had shallow inflow and a broad region of outflow. The stratiform region between the two eyewalls had lower reflectivities and was the only region where the vertically incident Doppler radar data seemed to show downward motion below the freezing level.

Gilbert's structure is compared with other intense Atlantic and eastern North Pacific hurricanes with MSLP >900 mb. Storms with lower MSLP have higher wind speeds in both inner and outer eyewalls, and wind speeds >50 m s^{-1} extend higher in storms with lower MSLP. Hurricanes Gilbert and Gloria (1985), the strongest Atlantic hurricanes yet analyzed by the Hurricane Research Division, had different outer eyewall structures. Gloria's outer eyewall had a deep region of inflow, while Gilbert's inflow layer was shallow. This may explain differences in the subsequent evolution of the two storms.

1. Introduction

The minimum sea level pressure (MSLP) of a tropical cyclone rarely falls below 900 mb. In the Atlantic basin reliable estimates of the MSLP of named tropical cyclones (those having sustained 1-min surface winds ≥18 m s^{-1}) have been available since 1944, the first year of routine airborne reconnaissance of tropical systems. From then through 1996 there were 522 named tropical cyclones [Neumann et al. (1993); and subsequent seasonal summaries from the National Hurricane Center (NHC, now called the Tropical Prediction Center)], but only two had an MSLP <900 mb: Hurricane Allen of 1980 (899 mb) and Hurricane Gilbert of 1988 (888 mb). Previously, the Florida Keys Labor Day hurricane of 1935 had an MSLP of 892 mb. Tropical cyclones of this intensity occur more frequently in the western North Pacific (WNP) basin than in the Atlantic. For example, from 1958 to 1985 crews on reconnaissance aircraft reported that 37 of the tropical cyclones in the WNP (8% of the total) had MSLP <900 mb (Joint Typhoon Warning Center 1958–85, hereafter JTWC).

Relatively little is known about the structure of tropical cyclones with MSLPs <900 mb. Jordan (1961) examined rawinsonde and flight-level data collected in the eyes of eight WNP typhoons with MSLP <900 mb. As these typhoons approached their most intense stages they had pressure falls >2.4 mb h^{-1} for at least 12 h, deepening more rapidly than Holliday and Thompson's (1979) threshold for ''rapidly intensifying'' typhoons (1.75 mb h^{-1}). At the time of the minimum MSLP, the eye diameter was <40 km, and the air in the eye was warm (700 mb temperatures >25°C in six of the eight cases) and often dry (relative humidity <50% in five of the eight cases). Later, as the MSLP began to increase, the air in the eye cooled and moistened.

The structure of less intense hurricanes and typhoons has been studied in greater detail. For example, Willoughby (1990) examined flight-level and radar data to determine the basic structure of hurricanes with maximum sustained winds >45 m s^{-1} and MSLP >900 mb. He concluded that these hurricanes usually have a convective ring outside the eyewall that contains a local

* Current affiliation: Tropical Prediction Center, NWS/NOAA, Miami, Florida.

Corresponding author address: Peter Dodge, Hurricane Research Division, Atlantic Oceanographic and Meteorological Laboratory, 4301 Rickenbacker Causeway, Miami, FL 33149.
E-mail: dodge@aoml.noaa.gov

maximum in tangential wind. Often the convective ring contracts, the eyewall weakens, the MSLP rises, and the convective ring becomes a new eyewall. Willoughby et al. (1982) referred to the convective ring as an outer eyewall and proposed that its contraction is part of a concentric eyewall cycle. WNP reconnaissance crews noted concentric eyewalls in 58% of the typhoons with MSLP <900 mb (JTWC), even though they were not required to report this pattern.

In one of the first descriptions of the vertical structure of strong hurricanes, Hawkins and Imbembo (1976) estimated wind fields in the intense stage of Hurricane Inez (1966) by combining flight-level data recorded at five different levels, from 950 to 150 mb. They showed a vertical ring of winds >50 m s^{-1} extending well above the 500-mb flight level. Flow into the eyewall was confined to some layer below 750 mb. Knowledge of the vertical structure of tropical cyclones was greatly enhanced after the Aircraft Operations Center (AOC) mounted a prototype airborne Doppler radar in the tail of one of the National Oceanic and Atmospheric Administration's (NOAA's) WP-3D research aircraft. Since the summer of 1982, the Hurricane Research Division (HRD) has collected airborne Doppler data with this radar during research and operational reconnaissance flights in several tropical cyclones and has developed techniques to calculate reliable wind fields throughout the troposphere, wherever there are sufficient radar scatterers.

Based on analyses of airborne Doppler radar velocity data, Marks and Houze (1987) described the three-dimensional wind field within 40 km of the center of mature Hurricane Alicia of 1983 (MSLP = 962 mb). These analyses showed that the radius of maximum wind (RMW) sloped outward with height and corroborated the outward slope of the RMW in composites of flight-level data (Willoughby et al. 1982; Jorgensen 1984a,b) and numerical simulations of hurricanes (Willoughby et al. 1984). Willoughby (1988) presented a conceptual model of the axisymmetric part of the core in which the radial and vertical motions define the secondary circulation. The radial motion is inward at low levels and outward in the upper troposphere, and the rising branch of the secondary circulation is located along the inner edge of the eyewall. The Doppler winds from Alicia provided the first observational evidence from a single tropical cyclone of the secondary circulation. The updraft cores, deduced from vertically incident Doppler radar data, occurred most frequently on the inner edge of the eyewall and tended to be strongest above 6 km.

Marks et al. (1992) analyzed Doppler data from a two-aircraft experiment in eastern Pacific Hurricane Norbert of 1984. Norbert's MSLP was 942 mb and the RMW sloped outward with height, but in contrast with Alicia, the maximum updrafts were at low levels and the radial flow was weak and outward below 5 km. The differences in the patterns of the radial flow and vertical velocity between Alicia and Norbert may be related to intensity change. Alicia was slowly strengthening but Norbert was weakening.

Franklin et al. (1993) incorporated airborne Doppler data in a kinematic analysis of Hurricane Gloria of 1985, one of the most intense hurricanes observed in the Atlantic basin. When the Doppler aircraft was in Gloria's eye, the hurricane had an MSLP of 919 mb, 3 mb higher than its lowest value. Gloria's three-dimensional wind structure differed somewhat from that in Alicia and Norbert, because the RMW did not slope outward with height below 500 mb, and the maximum wind was at 550 mb, well above the boundary layer. Franklin et al. suggested that the difference in the vertical structure of the vortex occurred because Gloria was in the early stages of a concentric eyewall cycle; inflow that resulted from subsidence inward of the outer eyewall caused tangential winds in the midtropospheric part of the inner eyewall to increase, thus reducing the slope of the RMW.

This paper presents analyses of data from a reconnaissance flight in Hurricane Gilbert on 14 September 1988, when its MSLP was ~895 mb, a few millibars higher than the minimum MSLP the previous day. The NOAA aircraft assigned to the mission had the prototype Doppler radar and recorded the first airborne Doppler radar data in a storm with MSLP <900 mb. The goal was to provide forecasters at NHC with information for operational warnings and prediction, rather than to record research data. Operational reconnaissance required flight tracks that were not optimal for postflight Doppler analyses, and the prototype Doppler data system did not record the Doppler velocities continuously. After the flight, the incomplete datasets from Gilbert's core were combined to estimate the axisymmetric components of the three-dimensional wind field. The analyses of the airborne Doppler data are compared with those of previously analyzed hurricanes and Willoughby's conceptual model of hurricanes with concentric eyewalls.

2. Storm history and the reconnaissance flight

Hurricane Gilbert developed from a tropical wave that was first identified in satellite imagery near the African coast on 3 September 1988 (Lawrence and Gross 1989). The wave became a depression and then a tropical storm on 9 September near Martinique and a hurricane south of Puerto Rico a day later. Gilbert devastated Jamaica as it moved west-northwestward across the northwestern Caribbean Sea, then strengthened rapidly, reaching its lowest MSLP to the east of the Yucatan peninsula. The hurricane crossed the northeastern part of the peninsula on 14 September, entered the Gulf of Mexico, and struck land for the final time on 16 September along the Mexican coast, about 220 km south of Brownsville, Texas. Gilbert killed 318 people and caused property damage estimated to be $5 billion (U.S.) throughout its lifetime; approximately $50 million of the damage was in southern Texas where outer rainbands spawned tornadoes.

Black and Willoughby (1992, hereafter BW92) described the eyewall replacement cycle in Gilbert, from the formation of the original inner eyewall on 11 September to its replacement by the outer eyewall on 16 September. In their discussion of data collected during a NOAA reconnaissance flight into Gilbert on 13 September, they showed that the sea level pressure deepened rapidly, 29 mb in 5.5 h, as the eyewall diameter contracted to 15 km and several rainbands formed a partial convective ring surrounding the eyewall, at radii about 60–70 km outside of the eye. Gilbert's lowest MSLP of 888 mb was an Atlantic basin record minimum (Willoughby et al. 1989) that was only 18 mb above the world record MSLP in Typhoon Tip (Dunnavan and Diercks 1980). The maximum 700-mb eye temperature was 27°C. The flight crew was unable to release any dropsondes but noted that the sea surface in the eye was clearly visible, indicating unsaturated air below flight level. The next reconnaissance flight, described in this paper, entered Gilbert's core on 14 September, about 8 h after the record low MSLP.

3. Data and analysis methods

a. Radar characteristics

The NOAA WP-3D aircraft flown on 14 September is equipped with lower fuselage (LF) and tail radars. The LF radar has a wavelength of 5.6 cm (5.3 GHz), scans horizontally at 3 rpm, and has a beamwidth of 1.1° in the horizontal and 4.1° in the vertical. The radar processor digitizes data out to 371 km, but the maximum ranges for qualitative and quantitative analyses are ~180 and 100 km, respectively (Marks 1985).

The tail radar scans at 10 rpm and usually rotates in a vertical plane normal to the flight track. The processor records reflectivity and the component of scatterer velocity along the radar ray derived from the Doppler phase shift, which we refer to as ''Doppler velocity.'' The wavelength of the tail radar is 3.2 cm (9.3 GHz) and the Nyquist velocity (the maximum unambiguous Doppler velocity recorded) is 12.88 m s^{-1}. The width of the elliptical beam is 1.9° in the plane of rotation and 1.35° in the plane perpendicular to it. At typical ground speeds of 125–150 m s^{-1}, rays at the same azimuth angle from consecutive sweeps are spaced 0.7–0.9 km along the flight track.

From 1982 to 1988, the prototype tail Doppler radar system processed and recorded the reflectivity and velocity data on separate systems. One data system recorded reflectivity within 92.6 km of the aircraft. The Doppler data system started digitizing at 0.9 km (the range delay) and a hardware error during the Gilbert flight limited reliable Doppler velocities to ranges <30 km from the aircraft, instead of the usual 78 km. Tape changes required 3–5 min, and various data problems caused other brief gaps in the coverage.

The aircraft carried a full complement of meteorological sensors and recorded flight-level information, for example, wind, thermodynamic, and navigational data, at 1-s intervals. AOC meteorologists provided postseason corrections for wind and navigation data that were used to unfold and map the Doppler velocities. Aircraft attitude angles (pitch, drift, and roll) and the tilt angle of the tail radar were corrected with algorithms similar to those of Testud et al. (1995). The adjustments were 0.7° for the roll angles, positive outbound and negative inbound, and 0.7° for the tilt angles.

b. Doppler analysis procedures

The pseudo–dual Doppler (PDD) analysis determines the three-dimensional kinematic structure of a hurricane by combining the Doppler velocities from a single aircraft for two successive radial passes (where a pass comprises inbound and outbound radial legs) with angular separation $>60°$ (Marks and Houze 1987). An interpolation routine first maps the Doppler data to a Cartesian grid centered on the storm's circulation, and a variational technique (Gamache 1997) then estimates the three-dimensional windfield.

Interpolation of Doppler data to a storm-centered grid requires an accurate storm track. The track was initially determined with storm positions from several LF sweeps and then smoothed with the polynomial method of Willoughby and Chelmow (1982). Storm-centered images were constructed from single radar sweeps by interpolating LF radar data to a Cartesian coordinate system that moved along the smooth storm track. In a time-lapse animation of the images the eye remained stationary, confirming that the track maintained the position of the eye in the center of the PDD domain. This track, only valid during the time of the flight, has a more northerly component than the best track based on smoothed 6-hourly positions in Lawrence and Gross (1989) and Neumann et al. (1993).

The reconnaissance flight includes only two consecutive radial aircraft penetrations suitable for PDD analysis of the inner eyewall. The analysis uses data from 0902 to 0909 UTC and from 1008 to 1016 UTC, when the aircraft was within 30 km of the center (Fig. 1). The other passes through the center have data gaps in the eyewall or turns in the eye. The Gilbert Doppler velocities were mapped on a $60 \times 60 \times 15$ km domain centered on the hurricane, with grid elements spaced 1.5 km in the horizontal and 0.5 km in the vertical. Because of the limited range of the Doppler radar data on this flight, Doppler rays from the two passes did not intersect at ranges >30 km from the center; therefore, the PDD analysis could not resolve the winds at those distances.

Gamache's (1997) variational algorithm estimates the three-dimensional wind field from all of the interpolated Doppler velocities that affect each grid point. The algorithm finds the velocity field that minimizes the sum of two weighted constraints. The first, most heavily weighted, constraint is that the velocity field should sat-

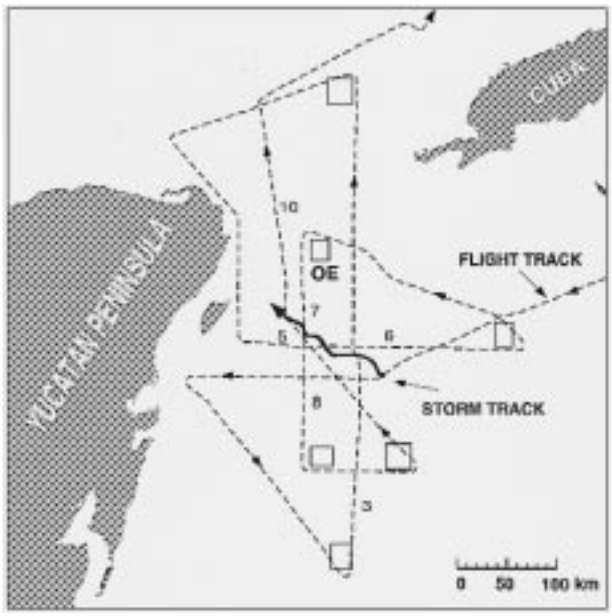

FIG. 1. Flight track on 14 September 1988. The solid line shows the hurricane track from 0609 to 1107 UTC. The dashed line is the flight track, with arrows indicating the aircraft direction. Cuba and the eastern coast of Mexico's Yucatan Peninsula are shaded in gray. Locations of Doppler analysis boxes are shown at turns; OE denotes the outer eyewall box discussed in section 4c. Numbered radial legs (inbound or outbound) are discussed in section 4c. Numbered radial legs (inbound or outbound) are discussed in the text.

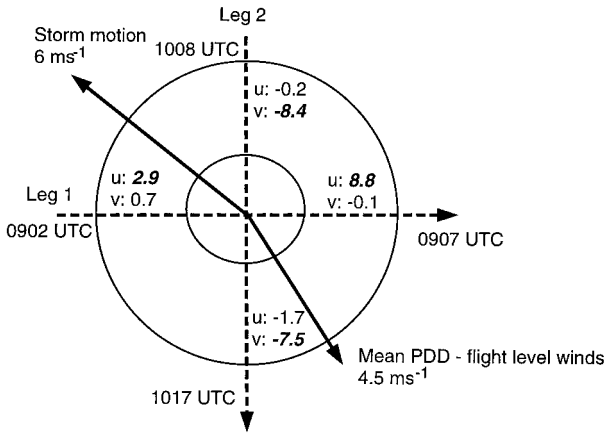

FIG. 2. Pseudo–dual Doppler (PDD) winds compared to flight-level winds. The dashed lines show the two flight legs of the PDD analysis, and the rings indicate the hurricane eyewall. The flight legs are labeled with start and end times for the PDD analysis. The mean difference in zonal (u) and meridional (v) winds are shown above or to the right of the flight segments, with values greater than zero indicating an excess in PDD winds. Components of the difference parallel to the flight legs are in bold, italic print.

isfy the equation of continuity as closely as possible. The second constraint is that the projections of the estimated wind on the radar rays should differ as little as possible from the Doppler velocities. Because the variational algorithm was formulated in cylindrical coordinates, the horizontal and vertical wind components were processed in a cylindrical coordinate system and then reinterpolated to the Cartesian grid for subsequent display. For the Gilbert analysis, the method includes more of the radar rays near the zenith angle and resolves the radial outflow better than an earlier iterative method that derived three-dimensional wind fields in the cores of Hurricanes Norbert (Marks et al. 1992) and Gloria (Franklin et al. 1993).

Radius–height cross sections of vertical velocities and reflectivities from the tail radar at vertical incidence were analyzed using the method described by Black et al. (1996). These two-dimensional cross sections are available along most of the flight track.

c. Representativeness of the PDD analysis

The wind at each grid point is based on two intersecting Doppler radar rays recorded ~1 h apart. The PDD analysis assumes a steady state for the average interval between the two flight legs. Willoughby (1990) analyzed data from several hurricanes and showed that the axisymmetric wind components at flight level in the eyewall varied slowly over several hours; therefore, an azimuthal average of the PDD analysis should provide a reasonable estimate of the axisymmetric components of the actual wind fields as a function of radius and height. Parrish et al. (1984) calculated the lifetimes of convective cells from WSR-57 radar reflectivity data in Hurricane Frederic (1979) and determined that only 4% of the cells could be tracked downwind for more than 15 min and <2% lasted more than 30 min. Thus, a convective-scale feature intersected by a Doppler ray during the first flight leg of a PDD pattern is unlikely to be the same feature intersected by a ray in the second leg of the pattern.

To evaluate the accuracy of the analysis, flight-level (2.8–3.0-km altitude) and PDD winds within 1.1 km of each other were compared. The mean difference between the two types of winds was a vector from 329° with a speed of 4.5 m s^{-1}. The mean storm motion at the time of the PDD analysis was toward 308° at 6 m s^{-1}. The near opposition of the two vectors is apparently a coincidental relationship. The storm motion's only effect on the PDD calculation is to position the Doppler velocities in the storm-relative coordinate system. Figure 2 shows that in each flight leg the cross-track components of the PDD and flight-level winds correlated more closely than the along-track components; the correlation coefficient between the flight-level and PDD analysis winds is 0.99 for the cross-track components and 0.70 for the along-track components. The cross-track flight-level and Doppler components were measured at the same time, but the along-track flight-level components were recorded an hour before or after the corresponding Doppler velocities. The difference is probably a combination of temporal evolution and unresolved navigational errors. The agreement is not as

good as that obtained by Marks et al. (1992) in Hurricane Norbert, where the wind components were <12 min apart. Nevertheless, the azimuthally averaged PDD windfield is likely to be within 5 m s^{-1} of the corresponding average kinematic wind structure that occurred in Gilbert's eyewall. The cause of the asymmetry of the differences, which are lowest west of the center (Fig. 2), is unknown. It may just be an artifact of the analysis, or it may mean that the winds on the western side of the eye changed less than in other parts of the storm.

Although the horizontal winds correspond well with the flight-level data, comparison of the vertical velocities shows that magnitudes of the maximum and minimum PDD were less than half of those from the vertical incidence Doppler data. Marks et al. (1992) and Franklin et al. (1993) point out that the temporal and spatial scales of PDD analysis preclude resolving convective-scale motions. Kinematic vertical velocities were based on divergence computed over areas >9 km^2 with time resolution >1 h. The PDD updrafts and downdrafts do correspond with mesoscale features and define the secondary circulation in the eyewall.

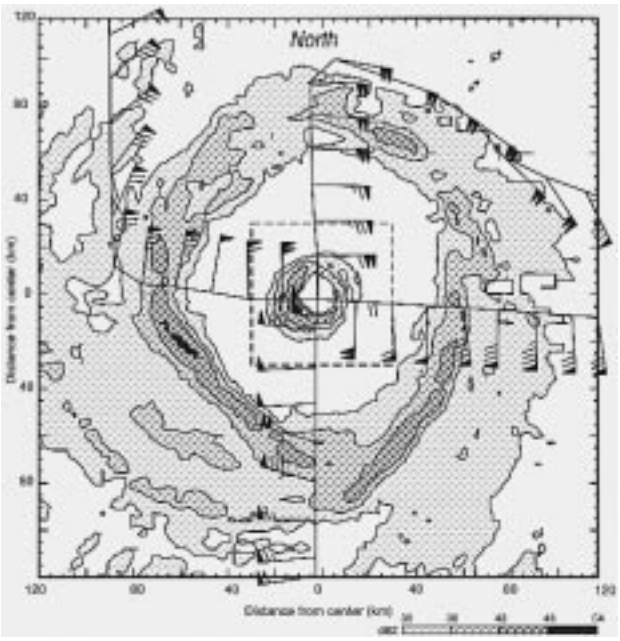

FIG. 3. Lower fuselage radar image from data collected 1008–1015 UTC 14 September 1988. The domain is 240 × 240 km, and the major tick marks are at 20-km intervals. Successively darker shading indicates radar reflectivities >30, 36, 42, and 48 dBZ. The small dashed box encloses the eye Doppler analysis domain. The line with the wind barbs is the flight track from 0858 to 1016 UTC. Wind barbs are plotted every 2 min, using the standard convention: a pennant is 25 m s^{-1}, a barb represents 5 m s^{-1}, and a half-barb is 2.5 m s^{-1}.

4. Results

The reflectivity pattern from a single sweep of the LF radar from the center of the storm shows the main features of Gilbert's structure in a 240 × 240 km domain (Fig. 3). The inner eyewall is the ring of reflectivity >30 dBZ located 10–20 km from the center that encloses the echo-free eye. The rainbands surrounding the eye at radii of 60–90 km form the outer eyewall, a ring of reflectivity >30 dBZ completely enclosing the inner eyewall and containing several embedded convective cells >36 dBZ. Between the inner and outer eyewalls is an annular area of low reflectivities, ≤30 dBZ, and stratiform precipitation. Other rainbands are beyond the outer eyewall, about 300 and 400 km from the center (not shown).

A radius–height cross section of tail radar reflectivity, averaged for the whole flight (Fig. 4), shows that the region beyond the outer eyewall consists mostly of stratiform rain. The mean height of detectable reflectivity (10 dBZ in Fig. 4) declines from 15 km in the inner eyewall to ~9 km beyond 150 km from the center. There is also a noticeable descent of the brightband altitude, from 4.8 km within 90 km of the center to 4.5 km outside of the outer eyewall.

a. The eye and inner eyewall

During this flight, the core of the storm changed little, and the MSLP remained near 895 mb. The eye (echo <25 dBZ at flight level) was ~15 km in diameter. BW92 pointed out that observations in the eye are consistent with Jordan's (1961) observations of intense typhoons past the time of peak intensity. The maximum 700-mb temperature in the eye was ~13°C, 7°C less than on the previous flight. A dropsonde sounding was saturated between flight level and the surface (Willoughby et al. 1989). However, in the lowest 25 mb the lapse rate was greater than moist adiabatic, suggesting less-than-saturated conditions. The tendency for saturated conditions below the cloud base, caused by the humidty sensor remaining wet, is a characteristic of Omega dropwindsondes and was pointed out by Franklin et al. (1988) in a discussion of a similar sounding in Hurricane Gloria (1985).

The flight-level tangential wind profile had two storm-relative speed maxima (Fig. 5). The primary maximum was in the inner eyewall, ~10 km from the center, and ranged from 60 to 74 m s^{-1} during the flight. On the first pass through the storm center, the strongest flight-level winds were in the north and west sides of the inner eyewall. About 4 h later, the maximum horizontal winds were on the south side. On the inner edge of the primary maximum the gradient of tangential wind averaged 7.8 × 10^{-3} s^{-1}, more than three times as large as the mean 2.0–2.5 × 10^{-3} s^{-1} that Samsury and Zipser (1995) found in a study of flight-level wind data in 20 hurricanes.

The largest updrafts at flight level in the inner eyewall were <5 m s^{-1} on the south side and 6–12 m s^{-1} on the north side. Maximum downdrafts were 2–7 m s^{-1} and tended to be stronger in the southern half of the eyewall. Analyses of the vertically incident Doppler ve-

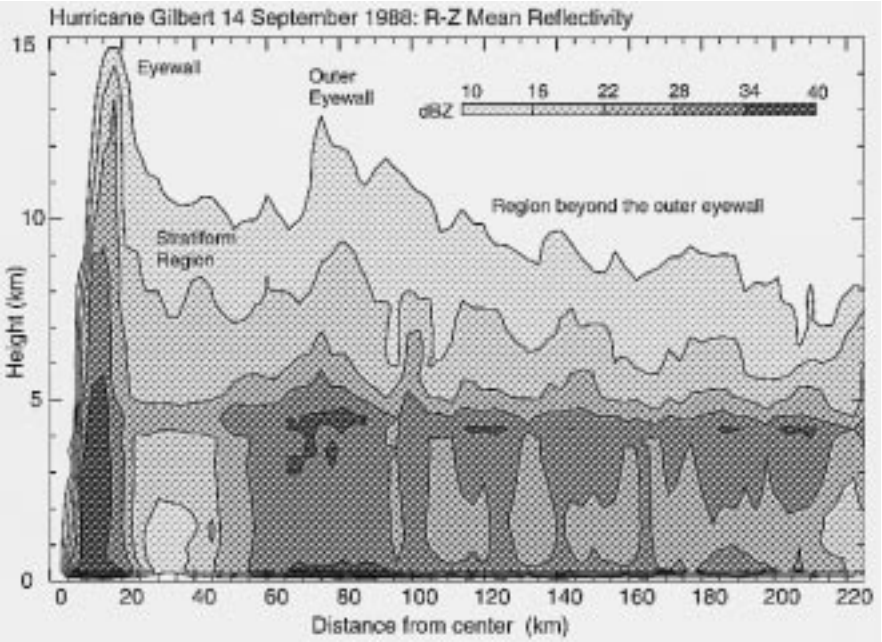

FIG. 4. Radius–height cross section of average tail radar reflectivity for the region within 225 km of the center of Hurricane Gilbert. Succesively darker shades of gray enclose areas with average reflectivity >10, 16, 22, 28, 34, and 40 dBZ.

locities from radial legs 5–8 (Fig. 1) indicate that maximum updrafts and downdrafts were ~26 and ~14 m s^{-1}, respectively, at altitudes near 10 km. Similar analyses by Black et al. (1996) showed that hurricane drafts are often stronger at altitudes near 12 km. Updrafts were concentrated in narrow regions along the inner edge of the eyewall (Fig. 6). Downdrafts were just radially outward from the updrafts in the western and southern parts of the eyewall, an asymmetric pattern also observed in other hurricanes (Black and Hallett 1986; Marks and Houze 1987; Marks et al. 1992; Black et al. 1996). Black et al. (1995) found in a preliminary analysis of 11 hurricanes (including Gilbert) the strongest upward motion upwind and the strongest downward motion downwind of the reflectivity maximum. This pattern was evident in Gilbert, where the reflectivity maximum was on the west side and the maximum updraft was found on the north (Fig. 6b).

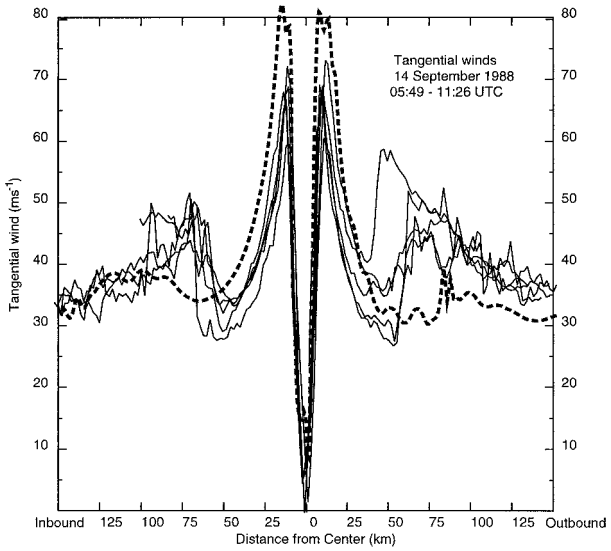

FIG. 5. Storm-relative flight-level tangential winds, plotted vs distance from storm center, for all legs during the reconnaissance flight on 14 September. Mean storm motion of 6 m s^{-1} from 128° was removed from the flight-level winds before plotting. Inbound legs are plotted on the left side of the figure and outbound legs are plotted on the right side. Maximum flight level winds on 13 September, 1744–2333 UTC, are indicated by the dashed gray curve. A mean motion of 6.6 m s^{-1} from 102° was subtracted from these winds.

A radius–height cross section of tail radar reflectivity from a single south–north radial pass (Fig. 7) shows the vertical structure of the precipitation. Strong reflectivities >40 dBZ were in a narrow core in the inner eyewall (10 km radius). Changes in the maximum height of the 20 dBZ contour in horizontal analyses of the tail radar reflectivity represent changes in the depth of the convection in the eyewall. The maximum height of the contour was >12 km initially and almost half the eyewall had reflectivities >20 dBZ at least 10 km in height (Table 1). On the last pass through the storm core ~5 h later, however, 74% of the echo tops >20 dBZ were 8 km or less. The decrease in height of the reflectivity maximum in the inner eyewall suggests a possible weakening of the convection that may have been in response to the strengthening of the outer eyewall (BW92).

The PDD analysis resolves both the primary (tan-

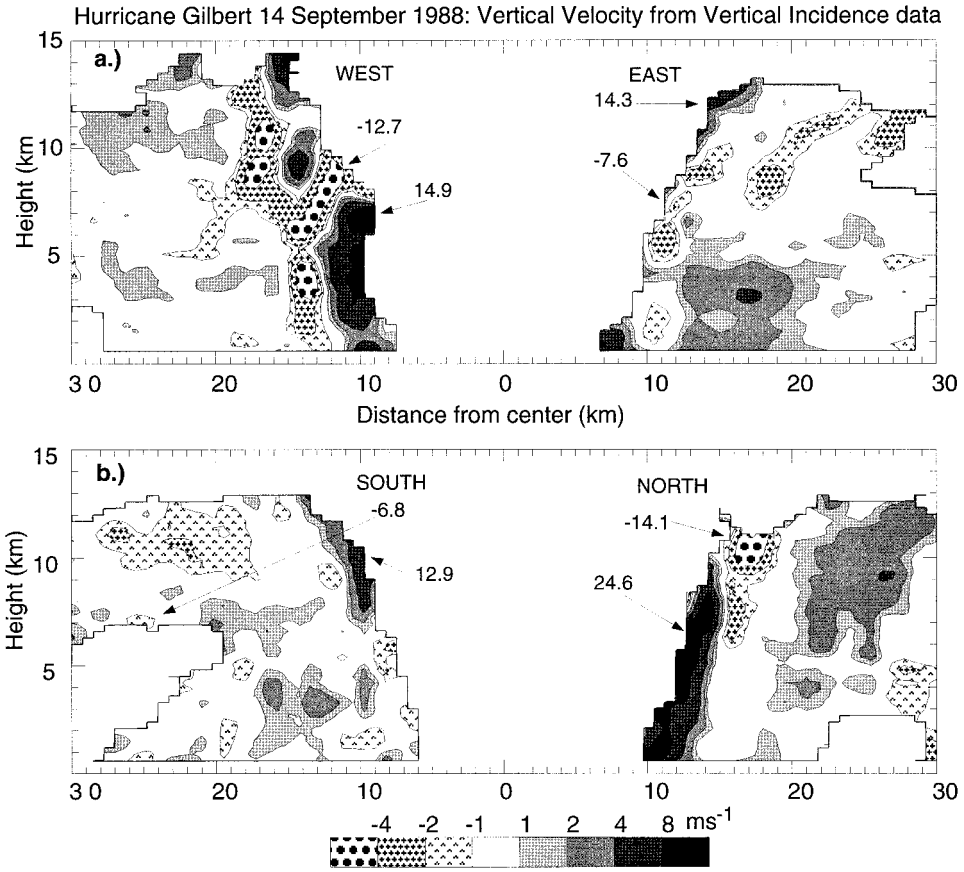

FIG. 6. Vertical velocity from vertical incidence Doppler data for (a) the east–west cross section through the eyewall, 0902:00 to 0909:00 UTC, and (b) the north–south cross section, 1008:00–1016:00 UTC. Upward vertical velocities are represented by increasingly darker shades of gray, and downward velocities are represented by increasingly denser stippled patterns. Arrows denote the maximum and minimum vertical velocities in each leg.

gential) and secondary (radial and vertical) flows of the tropical cyclone core. Azimuthal means of the tangential and radial flows as a function of radius and height were constructed from the analyses by averaging the velocities in rings relative to the mean center of circulation. The center was determined objectively by finding the 10–15-km wide annulus that maximizes the tangential circulation (Marks et al. 1992). An accurate center of circulation is necessary to compute the radial and tangential winds correctly. The mean center of circulation was 1.5 km east and 3.0 km north of the reflectivity center used to map the Doppler data in the PDD analysis. Figure 8 shows that the center of circulation varied <2 km with height. Similar small variations with height were found in Hurricanes Norbert (Marks et al. 1992) and Hugo (Roux and Marks 1996).

Figure 9 depicts the hodograph of the average horizontal winds in Gilbert within the ring 12–25 km from the center, averaged for each analysis level from 0.5 to 12.0 km altitude. This ring was selected for the averaging because the wind data were evenly distributed in the annular column up to 12 km in the PDD analysis. The hodograph only matches the storm motion near 11 km, although the winds are close to the storm motion from 6 km on up, and the vertically averaged mean wind was less than the storm motion. The range limitations of the Doppler domain restrict the Gilbert analyses to an area that is too small to give a mean wind that might correlate well with the storm motion. Franklin et al. (1993) determined that Hurricane Gloria's motion was most consistent with the vertically averaged mean wind computed in a domain of 65-km radius from the center, about 3.5 times the RMW in Gloria. The vertical shear of the horizontal wind is approximately perpendicular to the mean storm motion. In the lowest 10 km, the vertical shear of the wind is $\sim$7 m s^{-1} in Gilbert, but was about 10 and 15 m s^{-1} in Hurricanes Hugo and Norbert, respectively (Marks 1992; Roux and Marks 1996), and $\sim$13 m s^{-1} in Hurricane Gloria (Franklin et al. 1993). The smaller shear in Gilbert may explain why the center of circulation varied so little in the vertical in comparison with other hurricanes. Note that the slope of the individual centers from 3 to 8 km matches the direction of the shear.

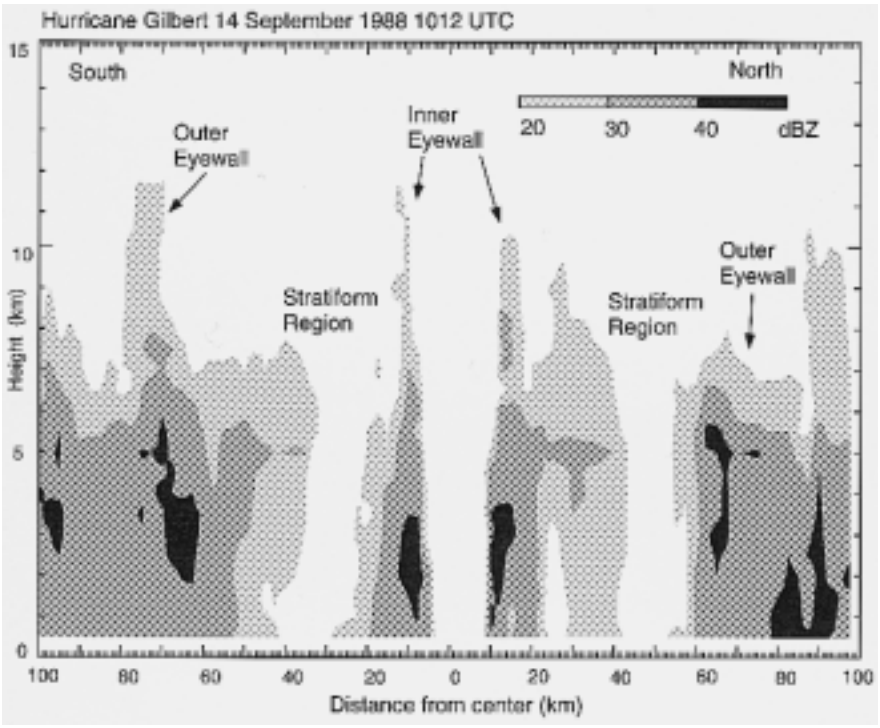

FIG. 7. North–south vertical cross section of tail radar reflectivity, centered on Gilbert's eye at 1012 UTC. Contours enclose areas ≥20, 30, and 40 dBZ (darkest).

Azimuthal averages of reflectivity, tangential velocity, and the secondary circulation are presented in Figs. 10 and 11. The reflectivity and tangential winds in the eyewall both decrease monotonically with height. [The vertical resolution of the PDD analysis is too coarse to resolve the low-level wind maximum detected near 1 km in other hurricanes (e.g., Powell et al. 1991)]. Mean tangential wind speeds >50 m s^{-1} extend to 12 km (Fig. 10), ~3 km higher than Hawkins and Imbembo (1976) estimated for Hurricane Inez of 1966 and Franklin et al. (1993) determined for Hurricane Gloria of 1985. Gilbert was more intense than those storms, so one would expect higher winds at similar heights, even if the wind structures were similar in all storms. The lower shear of the tangential wind at the RMW also contibuted to the elevated high winds (-1.31×10^{-3} s^{-1} in Gilbert vs -1.97×10^{-3} s^{-1} in Gloria). The reflectivity and tangential wind maxima both slope outward with height, but much less than has been observed in weaker hurricanes. The radar reflectivity maximum slopes 10° outward up to 8 km and then slopes 28° above that height. The tangential wind maximum slopes 18° outward. In contrast, in Hurricane Alicia both maxima sloped 46° from the vertical (Marks and Houze 1987). The tangential wind maximum is ~2 km outside the reflectivity maximum at altitudes up to 10 km and then is almost coincident with it above, a similar positioning to that

TABLE 1. Frequency of 20 dBZ echo heights, for all reflectivity within 30 km of center and >2.0 km in altitude.

Pass no.	<6 km %	6–8 km %	8–10 km %	10–12 km %	>12 km %
1	30	26	26	14	4
2	34	33	21	10	2
3	48	29	10	8	5
4	53	24	16	6	1
5	48	26	17	8	1

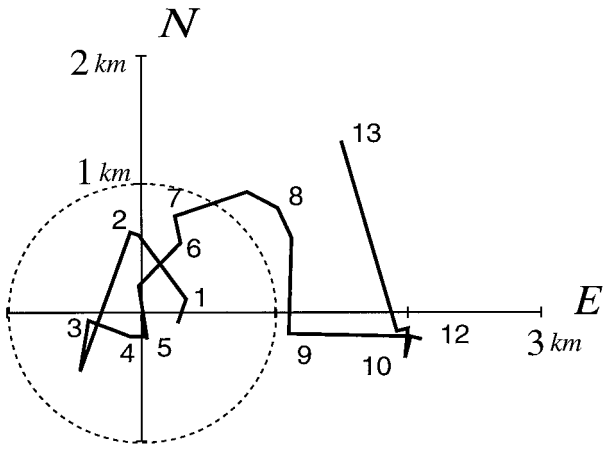

FIG. 8. Circulation centers at each level in the PDD analysis. Positions are plotted relative to the mean center of circulation in the first 6 km, which is 1.5 km west and 3.0 km north of the reflectivity center. The centers are plotted every 0.5 km in height and labeled every 1 km. The reference circle is 1 km in radius.

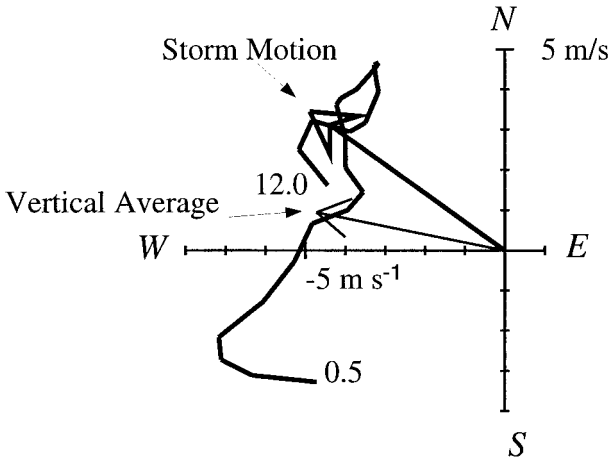

FIG. 9. Hodograph of mean winds from PDD analysis. Winds 12–25 km from the center were averaged for each level up to 12-km altitude. The hodograph is labeled at the first and last levels. Thick and thin arrows show the mean storm motion (from 0902 to 1016 UTC) and the density-weighted mean wind (vertical average), respectively.

observed in Doppler analyses of Hurricanes Alicia, Gloria, and Norbert. In contrast, Jorgensen's (1984a) composites of flight-level data from four hurricanes indicated that the RMW was *inside* the maximum reflectivity at lower levels and coincided with it at mid- to upper levels.

Kinematic vertical velocities in the eyewall were estimated from the horizontal wind components. The three-dimensional analysis resolves the locations of updrafts and downdrafts that satisfy the equation of continuity. The PDD vertical velocities vary from -7 to 8 m s^{-1}, less than half the magnitudes of the maximum convective drafts in the vertical incidence data. A core of upward motion >3.5 m s^{-1} is just inside the reflectivity maximum below 10 km and downward motion of -1 to -3 m s^{-1} is radially outward from the high reflectivities.

The axisymmetric PDD radial and vertical velocities show the secondary circulation (Fig. 11). The radial winds are inward at low levels and outward at higher levels. Just above the surface, inflow extends several

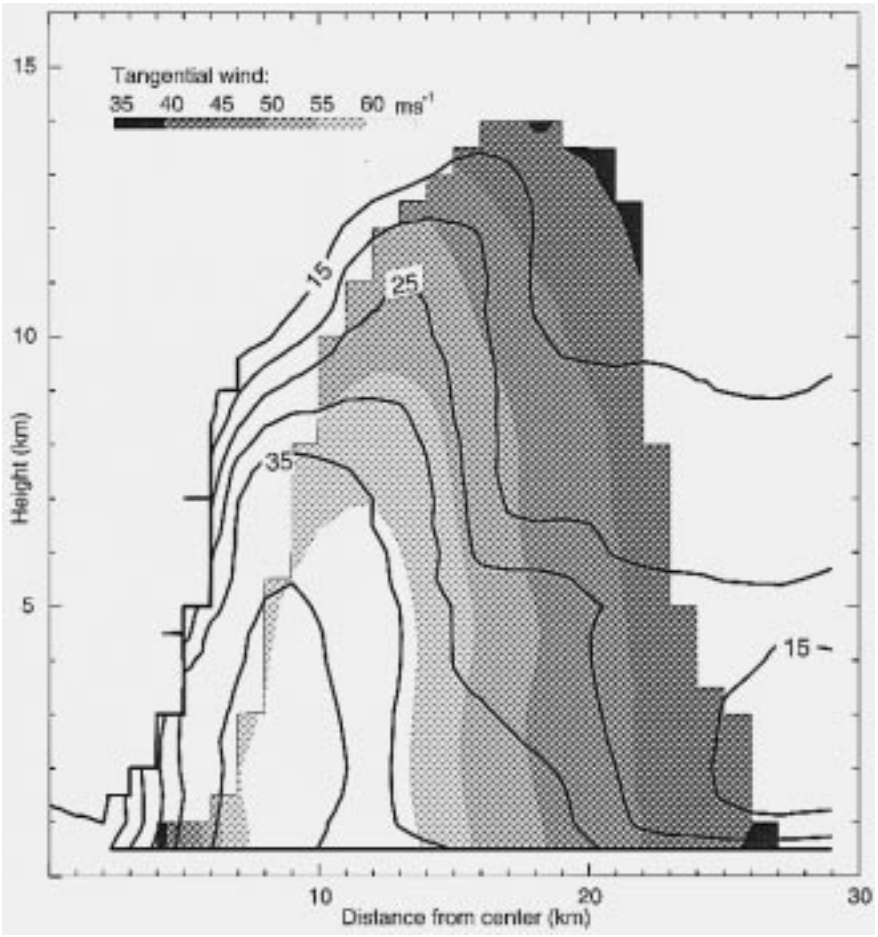

FIG. 10. Azimuthal mean tangential winds and reflectivity as a function of radius and height from the PDD analysis, for the period 0902–1016 UTC. Successively *lighter* shades of gray enclose higher wind speeds, starting at black for 35 m s^{-1}, in 5 m s^{-1} intervals. Solid lines are contours of reflectivity, in 5 dBZ steps starting at 15 dBZ.

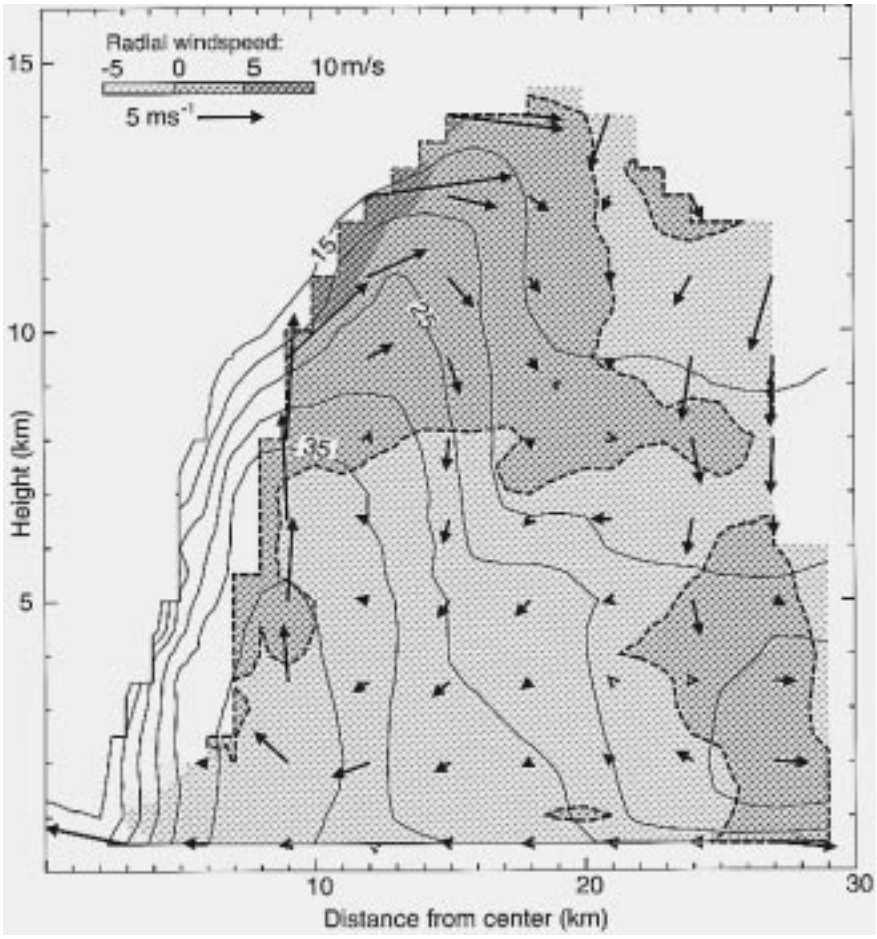

FIG. 11. Radius–height mean of the radial flow from the PDD analysis (0902–1016 UTC). Reflectivity (dBZ) is contoured as in Fig. 10, and the gray shades show the radial wind speed derived from the azimuthally averaged PDD analysis. Black arrows map the secondary circulation; the vertical component has been magnified two times to match the vertical scaling. The outflow regions are enclosed by a dashed line.

kilometers inward of the eyewall and may account for the high relative humidity in the eye, below flight level. The lack of suitable radar scatterers at higher altitudes precludes resolving the magnitude and altitude of the outflow just below the tropopause, outside of the eyewall.

The axisymmetric PDD winds can be used to estimate the degree of vortex balance by a simple pressure retrieval (described in the appendix), which assumes gradient balance of the radius–height mean winds. The retrieval technique calculates a surface pressure difference of 60 mb between the hurricane center and a radius of 30 km. The aircraft data system estimated surface pressure differences of 60 and 62 mb for the same spatial interval at 0906 and 1012 UTC, respectively. The aircraft procedure determines surface pressure as a function of the virtual temperature and the geopotential and pressure altitudes from standard atmospheric profiles between flight level and the surface (Merceret and Davis 1981). The agreement of the PDD and flight-level-derived pressure differences implies that the PDD windfield is very close to gradient balance. Willoughby (1991) analyzed the flight-level data from reconnaissance missions before and after this flight and also concluded that the lower-tropospheric portion of Gilbert's core (within 150 km of the center) was in gradient balance on timescales of ~6 h.

b. The stratiform region between the eyewalls

The area between the two eyewalls was about 10 times larger than the eye (Fig. 3). It contained stratiform precipitation, with reflectivities <30 dBZ, except in the bright band (Figs. 4 and 7), and flight-level winds of ~30 m s^{-1}. The average vertical velocities and their standard deviations, estimated from vertical incidence data (Fig. 12), were <1 m s^{-1} except in the vicinity of the bright band, between 4.5 and 5.5 km. The mean vertical motion was slightly upward above the bright band and downward below the bright band. Black et al.

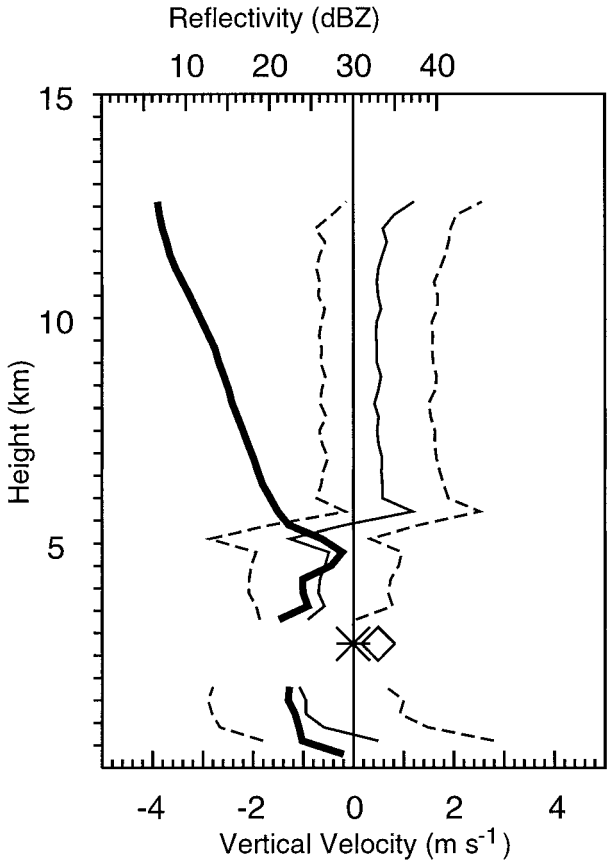

FIG. 12. Vertical profiles of average vertical velocity (thinner line) and reflectivity (thicker line), for the stratiform region from 30 to 55 km from the center of circulation. The average flight-level vertical velocity is denoted by a star and the diamond denotes the average of the absolute value of the vertical velocity. The dashed lines are plotted one standard deviation on each side of the vertical velocity plot.

(1996) calculated the average vertical velocity as a function of height in stratiform regions outside of the eyewall of seven hurricanes and determined a distribution resembling that shown in Fig. 12. Marks and Houze (1987) and Black et al. (1996) pointed out that the vertical structure of the velocity pattern in the stratiform region is similar to the mesoscale up- and downdraft pattern in the trailing stratiform regions of tropical squall lines (e.g., Houze and Hobbs 1982).

The magnitude of the downward motion in the layer below the bright band may have been slightly overestimated. The aircraft flew ~2 km below the bright band in this region. The average of the absolute values of flight-level vertical velocity was <0.5 m s^{-1} (Fig. 12), with standard deviation <0.5 m s^{-1}, but the mean Doppler-estimated wind speed was ~1 m s^{-1} downward, above and below flight level. Black et al. (1996) discuss the difficulty in estimating vertical velocities in light rain, where uncertainties in fall speeds estimated from bulk formulas are greater than the magnitude of the air

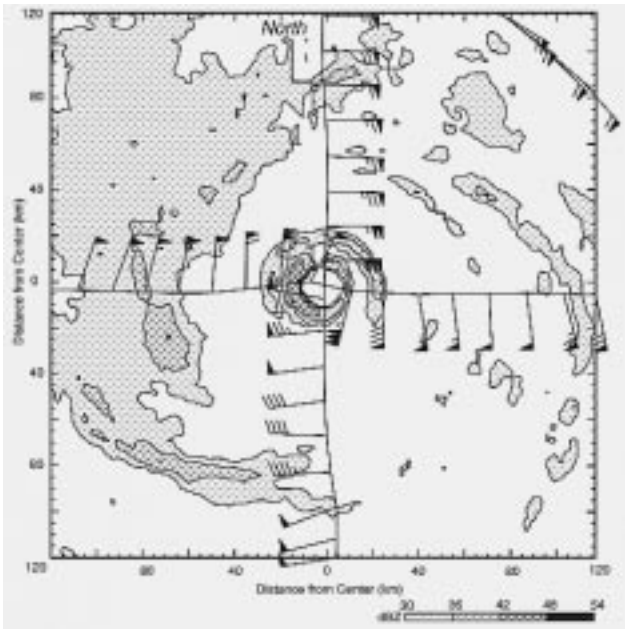

FIG. 13. Lower fuselage radar image from data collected 2150–2152 UTC 13 September 1988. Scaling and shading are the same as in Fig. 3. The flight track is from 2016 to 2210 UTC.

motions themselves. Nevertheless, both the flight level and Doppler data indicate that the vertical motions in this region were weak.

c. The outer eyewall

During the preceding reconnaissance flight, the precursor of the outer eyewall was a semicircular convective ring that was open on the eastern and southeastern sides (Fig. 13). Reflectivities >30 dBZ increased (Fig. 3), but the outer eyewall reflectivity was not as convective as the inner eyewall on 14 September. To compare the precipitation distributions in the two eyewalls, composite analyses of tail radar reflectivity were separated into convective and stratiform regions by the technique of Steiner et al. (1995), and then distributions of water mass were estimated from the reflectivity using the same relationships as Gamache et al. (1993) used to construct the water budget in Hurricane Norbert. In the inner eye region, 75% of the water mass was in the convective region (which composed 43% of the area covered by echo), but only 52% of the outer eyewall's water mass was in convective regions (which composed 35% of the echo area). A plot of the distributions (Fig. 14) shows that the peak in the convection was about 5 dBZ greater in the inner eyewall. Marks et al. (1993) determined a similar difference in the inner and outer eyewalls of Hurricane Anita (1977), although they did not differentiate between convective and stratiform precipitation. In their analysis, though, the difference was found in distributions of rain rates computed from in situ microphysical data.

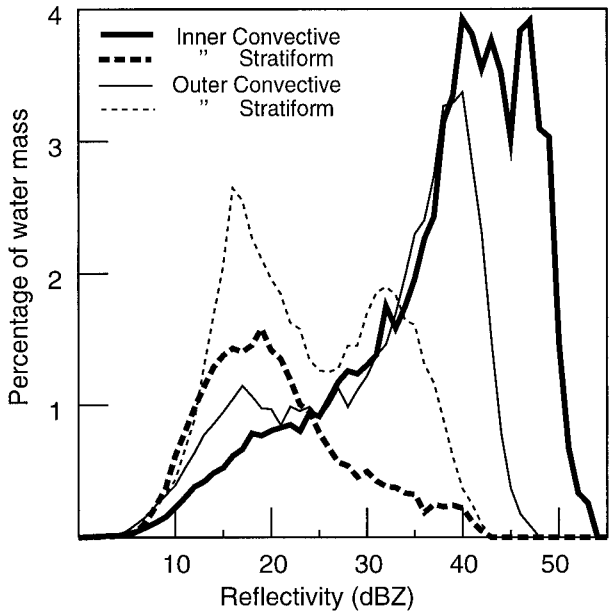

FIG. 14. Frequency distribution of water mass estimated from radar reflectivity in the layer from 1.5–15 km. The thick solid and dashed lines show the distribution (in percent of total water mass) of convective and stratiform precipitation in the inner eyewall region, from 0 to 30 km in radius, in 1 dBZ steps. The thin solid and dashed lines show the same distribution for the outer eyewall region, from 55 to 85 km in radius.

The horizontal reflectivity structure in the outer eyewall evolved from a series of short convective and stratiform rainbands in a quasi-circular pattern to a closed ring of echo >36 dBZ. At 0606 UTC, the outer eyewall consisted of several rainbands at distances of 65–90 km from the reflectivity center, in a roughly circular arrangement (Fig. 15a) that persisted until ~0840 UTC, when a linear rainband formed in the northeast part of the outer eyewall. The midpoint of this band was ~50 km from the center (Fig. 15b) and its development gave the outer eyewall an oblate shape. This change in shape possibly occurred when the hurricane's motion shifted from toward 278° to 325°, one of several track oscillations that is smoothed out of the best track as given in Neumann et al. (1993). Muramatsu (1986) described a similar pattern of track changes associated with linear features in an outer rainband in a typhoon near Japan in 1980. The Gilbert rainband maintained its linear shape as it rotated around the center, and by 1010 UTC it was in the southwest part of the storm (Fig. 3), where it was almost perpendicular to another band. A similar reflectivity pattern also occurred during the landfall of Hurricane Alicia (1983) (Dodge et al. 1987). At 1109 UTC the reflectivity center was 50 km from the northeast part of the outer eyewall (Fig. 15c) but ~70 km from the southern and western parts. The outer eyewall asymmetry developed during another track change, from toward 341° to 295° at 1040 UTC. It is not clear

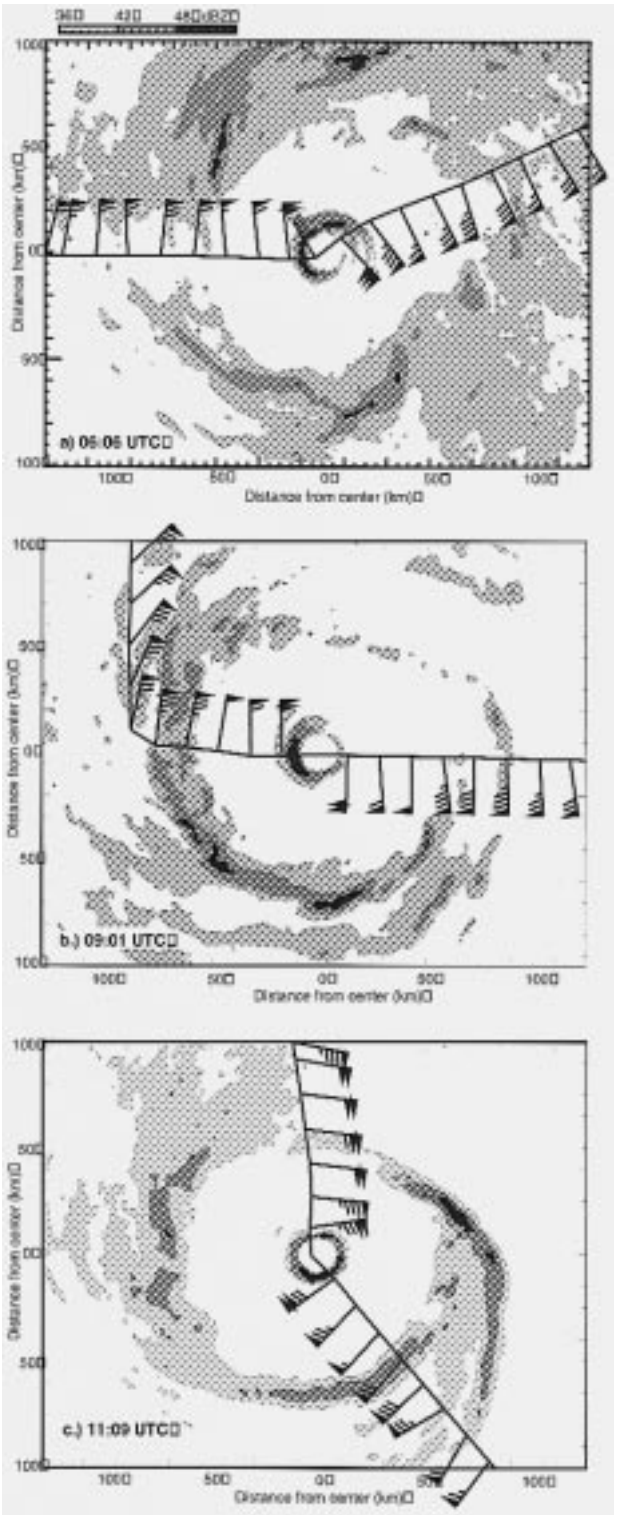

FIG. 15. Lower fuselage PPI displays from times when aircraft was near center of Hurricane Gilbert. Domain is 256 × 200 km. Successively darker shades of gray enclose areas with reflectivity >36, 42, and 48 dBZ. Flight-level winds are plotted every 2 min, as in Fig. 3; (a) 0606, (b) 0901, (c) 1109 UTC.

whether the changes in the outer eyewall structure caused or were caused by the track changes.

The secondary flight-level wind maximum (Fig. 5) was 45–50 m s^{-1} and much broader in radial extent than the primary wind maximum in the inner eyewall. The maximum was 60–80 km from the center, near the inner edge of the outer eyewall (BW92) and was more pronounced than during the previous flight (see dashed curve in Fig. 5). Flight-level winds were highest in the northern bands, but the maximum reflectivity in the outer eyewall was generally in the southern sector after 0600 UTC (Fig. 15), similar to the inner eyewall.

Samsury and Zipser (1995) used flight-level data collected in 20 hurricanes to study secondary horizontal wind maxima (SHWM). They found that the mean radial gradient of tangential wind was $\sim 6 \times 10^{-4}$ s^{-1} in the 10 km radially inward from the SHWM (their Fig. 4). They also remarked that Hurricane Gilbert had ''extremely peaked'' profiles of tangential wind in both inner and outer eyewalls. Indeed, the gradient of tangential wind in the flight-level data in Gilbert's outer eyewall on 14 September averaged 1.3×10^{-3} s^{-1}, twice the mean gradient of Samsury and Zipser. In individual passes 3, 8, and 10 (Fig. 1) the outward increase in tangential winds was $>2 \times 10^{-3}$ s^{-1}, similar to the mean gradient of $2–2.5 \times 10^{-3}$ s^{-1} for the inner eyewall reported by Samsury and Zipser. They also showed that the SHWM in Gilbert was located in the outer eyewall rainbands (their Fig. 12), as was the case in ~75% of the SHWM in their sample.

Black and Willoughby (1992) indicated that the outer eyewall was fully developed on 14 September, and the SHWM continued to contract during the flight. However, examination of the individual flight-level profiles shows that contraction of the SHWM occurred only in the northern part of the outer eyewall (Fig. 16a). The increase of flight-level tangential wind there, from 45 to 60 m s^{-1}, is consistent with conservation of angular momentum. The northern part of the outer eyewall appeared to contract ~20 km during the flight, but this can be explained by the eccentricity of the outer eyewall and the rotation of the linear convective feature until it was north of the eye. The angular momentum at the radius of the maximum wind in the outer eyewall at 0750 UTC was equal to the angular momentum at the radius of the maximum wind at 1126 UTC (Fig. 16b). This contraction and increase in wind apparently was a transient that had little effect on the outer eyewall radius in general though, because 24 h later on 15 September, after Gilbert had crossed the Yucatan Peninsula, the mean wind maximum of 40 m s^{-1} (now the RMW since the inner eyewall had dissipated) was still ~65 km in radius (Fig. 4d in BW92).

PDD analysis of one portion of the outer eyewall shows some features of the secondary circulation there. Radial legs during hurricane reconnaissance flights usually extend 150 km or more from the center of the storm (Willoughby 1990), but during the later part of the Gilbert flight some legs were shortened so that the aircraft could complete the five center fixes requested by NHC. Fortunately for the analysis, the aircraft turned just outside the outer eyewall at 0959 UTC, ~100 km north of the center, to start the fourth inward pass. Before turning toward the south the aircraft had been on a downwind leg toward the west-northwest that was just outside the region of higher reflectivity in the outer eyewall (Fig. 3). The tail radar data collected before and after the turn provide Doppler velocities for a three-dimensional analysis in an area representing ~3% of the outer eyewall. The winds in the analysis box are from 74 to 96 km from the center of the storm.

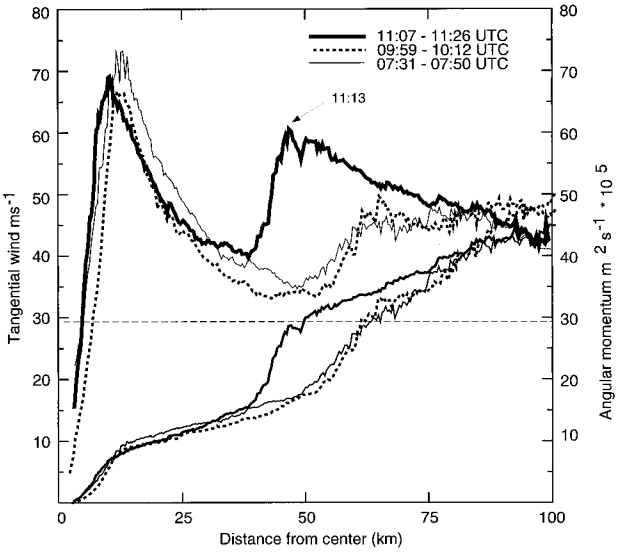

FIG. 16. Flight-level winds and angular momentum in legs that passed through northern portions of inner and outer eyewalls. The upper set of curves depict the flight-level tangential winds. Thin, dashed, and thick curves are for data ending at 0750, 1012, and 1126 UTC, respectively. The lower set of curves show the absolute angular momentum, in units of 10^5 m^2 s^{-1}. Dashed horizontal line indicates the angular momentum of the tangential wind maximum of the outer eyewall at 1113 UTC.

Animation of LF radar data from 0951 to 1003 UTC revealed that coherent reflectivity maxima moved through the analysis region with speeds of 46 m s^{-1} toward 283° (storm relative). The advection speed of the maxima was used to position the Doppler data, to preserve any cellular patterns of divergence in the band (Powell 1990). Two cores of reflectivity >40 dBZ reached altitudes of 3 km. Peak winds of 56 m s^{-1} were calculated in the northeast corner of the box, which agree with the flight-level winds and confirm that this region included the secondary wind maximum. Tangential winds >40 m s^{-1} extended to 10 km (Fig. 17a).

The flow toward the storm center was confined to a shallow layer <2 km (Fig. 17b), and outflow occurred everywhere above that level. Barnes and Powell (1995) examined data collected on 12 September in one of Gilbert's rainbands ~175 km southeast of the center.

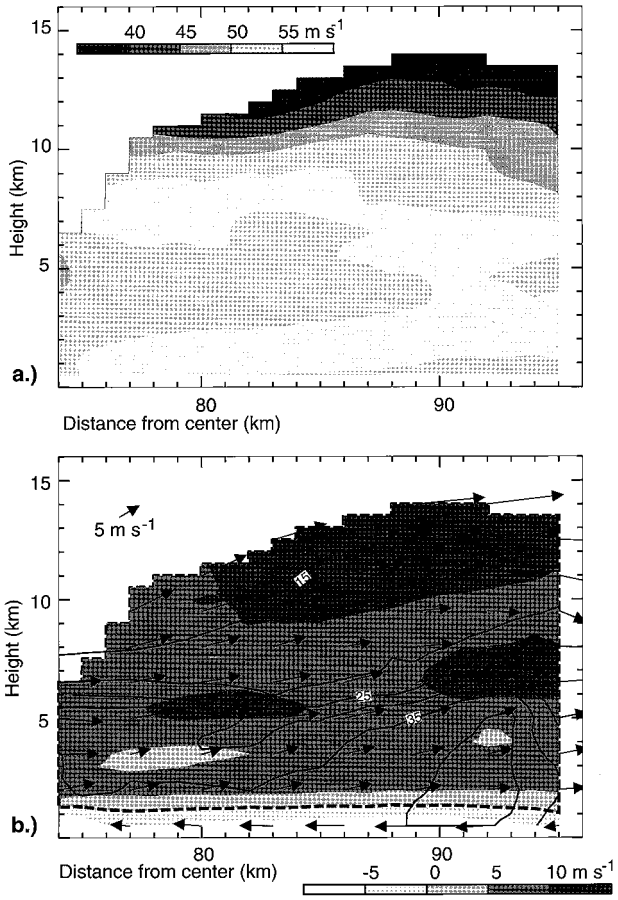

FIG. 17. (a) Radius–height mean tangential wind in outer eyewall analysis box. Successively darker gray shades indicate increasing speeds in 5 m s^{-1} increments, starting at 35 m s^{-1}. (b) Radius–height means of the radial wind and reflectivity box. Gray shades denote radial flow and the bold dashed line seperates inflow (lighter shades) from outflow (darker shades). The contour lines show reflectivity in 5 dBZ increments, starting at 15 dBZ.

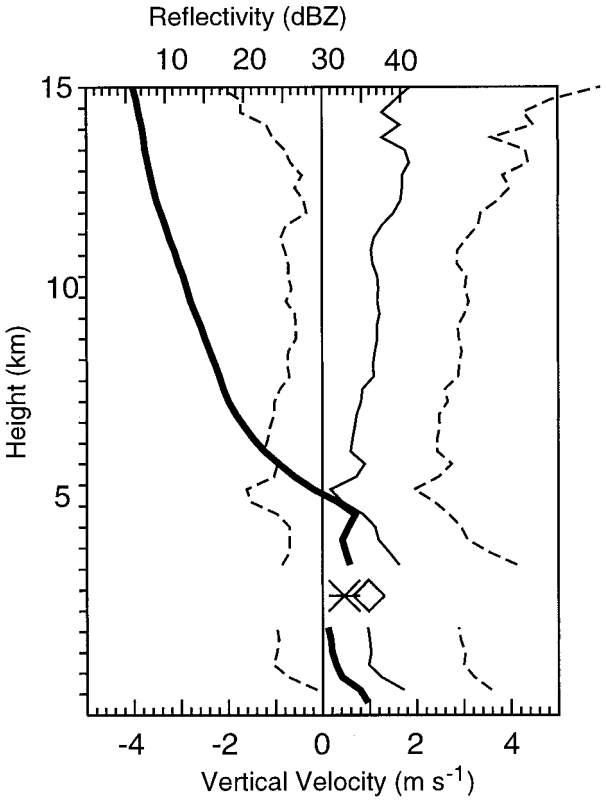

FIG. 18. As in Fig. 11 except that the area is 55–90 km from the center of circulation.

Their Doppler analysis also showed radial inflow only in a shallow layer. At least in this part of the outer eyewall, the structure of the secondary circulation was more similar to that in the rainband described by Barnes and Powell than in Gilbert's inner eyewall. The PDD vertical velocities were weak ($\pm$1–2 m s^{-1}) and predominantly upward except for those outside the reflectivity core in the upper troposphere, as were those from the vertical incidence data for the legs that bracket the domain.

The average vertical velocity from the vertical incidence data in the outer eyewall was $\sim$1 m s^{-1} upward at all levels (Fig. 18). The maximum updrafts and downdrafts in the outer eyewall were weaker than those in the inner eyewall. The strongest updrafts, $>$7 m s^{-1}, were on the south side of the eyewall. These were located in cores of higher reflecivity that were at times higher than some regions of the inner eyewall (e.g., Fig. 7). When the aircraft crossed the outer eyewall on the last flight leg into the eye (Fig. 15c), it passed through two rainbands that had distinct updraft cores with vertical velocities $>$7 and 4 m s^{-1}, respectively. The southern part of the outer eyewall was the only place with a pattern of downdrafts occurring radially outward from the updrafts, as in the inner eyewall. Other parts of the outer eyewall seemed to have less intense updrafts. Black et al. (1996) pointed out that well-organized up- and downdrafts are most often found only in the inner eyewall.

d. Beyond the outer eyewall

The region beyond the outer eyewall was not as well sampled as areas closer to the center of the hurricane, but the flight legs did extend at least 200 km in all quadrants and $\sim$280 km to the north and northwest (Fig. 1). The envelope of hurricane-force winds ($\geq$33 m s^{-1}) extended 170–200 km, at least 70 km farther from the center than in Hurricane Gloria [Fig. 7 in Franklin et al. (1993)]. About 280 km north of the center flight-level winds were 35 m s^{-1}, an indication of the large horizontal extent of Gilbert's circulation. In comparison, Weatherford and Gray (1988) studied 66 WNP typhoons that occurred from 1980 to 1982 and found that, on average, hurricane-force winds only extended $\sim$100 km (1° latitude) from the center in typhoons with MSLP

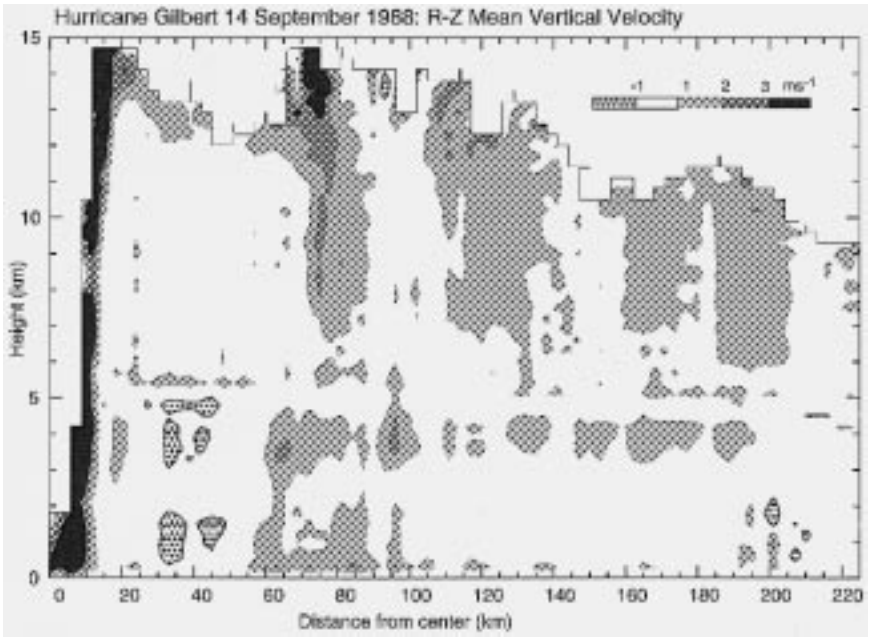

FIG. 19. Radius–height cross section of average vertical velocity for the region within 225 km of the center of Hurricane Gilbert. Upward vertical velocities are indicated by successively darker shades of gray, with black enclosing areas ≥ 3 m s^{-1}. The white area comprises weak vertical velocities from -1 to 1 m s^{-1}, and the stippled regions enclosed by the black contour line have vertical velocities < -1 m s^{-1}.

<920 mb. Similar statistics have not been compiled for the Atlantic basin.

The atmosphere within the region bounded by the outer eyewall was warmer than the air outside, consistent with an elevated bright band. The flight-level data show equivalent potential temperatures (θ_e) of 355 K at 700 mb inside of the outer eyewall, ~5 K warmer than in the stratiform region between 100 and 150 km from the storm. At radii of 200 km, the flight level θ_e of 342 K at 700 mb matches the θ_e in soundings from Belize and Merida taken at 1200 UTC 14 September. The 0° isotherm was at 4.7 km elevation in 0600 UTC soundings at Merida and Belize, somewhat lower than the 4.9 km in Jordan's (1958) mean hurricane-season sounding for the West Indies. A brightband height of 4.8 km inside of 200 km is more consistent with a 0° isotherm at 5.1 km or higher, because the enhanced reflectivity usually peaks about 300 m below the 0° isotherm (Austin and Bemis 1950).

The region beyond the outer eyewall was characterized by weak vertical velocities (Fig. 19). The average profile of vertical velocity above flight level (Fig. 20) is similar to those for the inner and outer eyewalls, with upward motion of 1–2 m s^{-1} above 3 km. Below the flight level, however, the upward motion is only about 0.5 m s^{-1}, except where the aircraft passed though rainbands 180 km east of the center. The difficulty in estimating vertical velocities in light rain also applies in this region, where uncertainties in estimated fall speeds can be greater than the magnitude of the air motions (Black et al. 1996).

5. Conclusions

The airborne Doppler radar data from the reconnaissance flight in Hurricane Gilbert on 14 September 1988 were the first ever collected in a tropical cyclone with MSLP <900 mb. Gilbert had deepened rapidly the day before, and the cloud structure and temperature in the eye were consistent with a storm past peak intensity (BW92). Although the MSLP was 7 mb higher than its record minimum on 13 September, the MSLP did not increase during the flight.

The most striking feature in the PDD analysis of the inner eyewall was the vertical extent of tangential winds >50 m s^{-1} to 12 km, ~3 km higher than had been previously reported. Even though the storm was past the time of peak intensity, the pressure gradient had not weakened appreciably in the core and strong winds were maintained at these heights.

Radar reflectivity identified a stratiform region between the inner and outer eyewalls that was relatively free of rain. Flight-level observations showed that it contained minima in tangential winds and weak vertical velocities. The vertical incidence Doppler data from the region indicated that, on average, there was weak upward and downward motion above and below the bright band, respectively. This was the only region that had

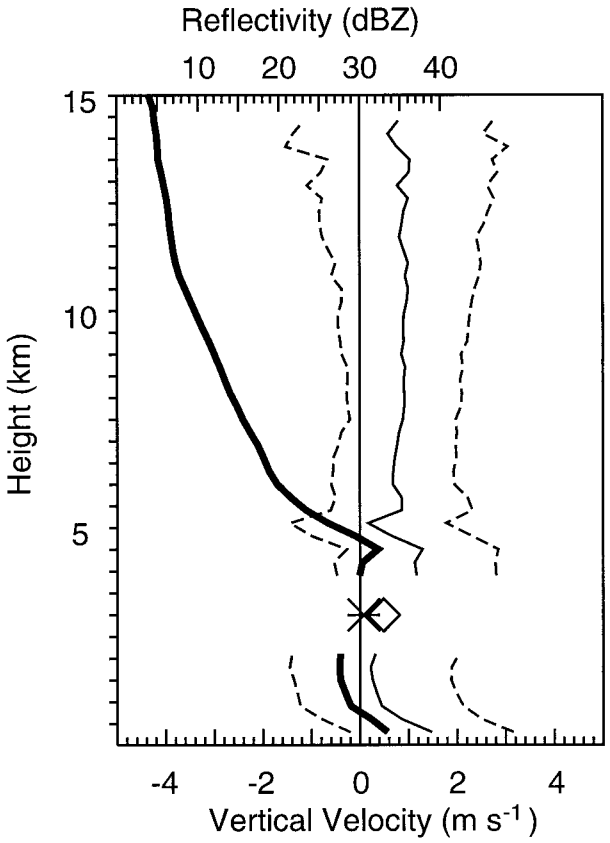

FIG. 20. As in Fig. 11 except that the area is 90–200 km from the center of circulation.

average downward velocity below the bright band, a feature that is characteristic of mature mesoscale convective systems (BW92; Houze and Hobbs 1982).

The outer eyewall evolved during the flight into a closed, oblate ring with embedded convection. The outer eyewall precipitation was only ~52% convective, however. Oscillations in the motion of the eye may be related to the changes in the orientation of the rainbands that composed the outer eyewall. This was also the first time that Doppler data were collected in an outer eyewall in such a way that PDD analysis was possible. In a small portion of the outer eyewall there is an inflow–outflow structure similar to that in one of Gilbert's outer rainbands two days earlier (Barnes and Powell 1995). However, the convection in this part of the outer eyewall was shallower. The radial flow may be different in areas where the outflow is confined to the upper levels of the troposphere, the tangential wind gradient is sharper, and the convection is deeper, that is, those regions that are more similar to the inner eyewall.

The region beyond the outer eyewall consisted largely of stratiform rain and a few areas with convective rainbands. The average vertical velocity distributions were more similar to the inner and outer eyewalls than to the stratiform region between them, which probably reflects the inclusion of convective updrafts in the statistics. The bright band was lowest in this region, closer to the environmental average (deduced from soundings).

Table 2 compares Hurricane Gilbert with three other strong Atlantic and eastern Pacific hurricanes that were monitored by aircraft with airborne Doppler radar and analyzed by HRD. The sample size is small, but a few features may be representative of strong tropical cyclones. The depth of tangential winds >50 m s^{-1} increases with intensity (MSLP). Norbert and Alicia only had winds of this magnitude up to 3 km, while Gloria and Gilbert's strong winds extended much higher. This difference in height of the strong winds is not just a result of stronger winds at the surface, because the vertical shear of the tangential wind was also weaker in the stronger storms. For example, if the shear in Alicia had been that of Gilbert, 50 m s^{-1} winds would have

TABLE 2. Characteristics of hurricanes studied by the HRD. Included are hurricanes with pseudo–dual Doppler analyses.

	Gilbert[a] 14 Sep 1988	Gloria[b] 24 Sep 1985	Norbert[c] 25 Sep 1984	Alicia[d] 18 Aug 1983
MSLP (mb)	895	919	952	967
dP (mb h^{-1})	~0.0	−2.5	+2.0	−1.0
Flight level:				
RMW (km)	9	19	26	12
V max (m s^{-1})	76	67	50	53
W max (m s^{-1})	11	17	6	3
Vertical structure:				
30 dBZ height (km)	8.5	13.5	7	5
Height $V > 50$ m s^{-1} (km)	12.5	8	3	<3
Tangential wind shear at RMW (s^{-1})	−0.00131	−0.00197	−0.00219	−0.00297
Outer eyewall:				
radius (km)	70	100–125	n/a[e]	40–60
V max (m s^{-1})	60	40	n/a	45

[a] Black and Willoughby (1992).
[b] Franklin et al. (1993); Willoughby (1990).
[c] Marks et al. (1991).
[d] Marks and Houze (1987); Willoughby (1990).
[e] Norbert had completed a concentric eyewall cycle prior to the flight summarized here.

extended to 10 km, instead of 3 km. The depth of reflectivity >30 dBZ is not well related to the MSLP or the depth of maximum winds >50 m s^{-1} (Table 2), but the depth of stronger reflectivity may be related to the stage of the eyewall evolution. Gloria's pressure was still dropping and the deep convection was helping to maintain a strong warm core at upper levels, which implies a decrease in gradient wind with height. In Gilbert the pressure had stopped falling, and the warm core may have cooled in the upper levels, with a correspondingly weaker radial temperature gradient, in which case the gradient wind would decline less with height.

Hurricanes Gilbert, Gloria, and Alicia all had outer eyewalls during the analysis periods [Norbert had completed an eyewall replacement cycle prior to this flight (Marks et al. 1992)]. The maximum flight level winds in the outer eyewall were strongest in Hurricane Gilbert. However, Gloria's outer eyewall was 30–55 km farther from the center than Gilbert's outer eyewall, and the winds would have been stronger at a radius similar to Gilbert's, by conservation of angular momentum. In that sense, Alicia's outer eyewall had the weakest winds, 45 m s^{-1} only 40–60 km from the center. In this small sample, storms with lower MSLP had stronger wind speeds in the outer eyewalls. Franklin et al. (1993) found inflow through a deep region at the radius of the outer eyewall in Gloria, but in the limited region of Gilbert's northern outer eyewall presented here, the inflow layer was quite shallow and the outflow layer was deep.

Gilbert had achieved its peak intensity ~12 h before (BW92) and Gloria's pressure began to rise ~2 h after the time of the PDD analysis (Franklin et al. 1988). In the 36 h following the PDD analysis time, for both storms, the MSLP increased and the maximum winds in the inner eyewall decreased, by 20 m s^{-1} in Gloria and 30 m s^{-1} in Gilbert (BW92; Willoughby 1990). In 36 h the two storms moved through different environments; Gilbert crossed the Yucatan Peninsula, but Gloria stayed over open water. Yet in both storms the outer wind maxima changed little, remaining at ~40 m s^{-1}.

More research is neccessary to describe the changes in the kinematic structure as a ring of convective rainbands evolves into an outer eyewall. HRD plans to collect more data in well-defined outer eyewalls, during future research or reconnaissance flights, to resolve the three-dimensional wind fields in both convective and stratiform regions. In the future, the PDD analyses from Gilbert will be compared with analyses from other storms in different parts of the eyewall cycle.

Acknowledgments. The AOC flight crew helped to collect the radar and flight-level data, and the AOC scientific staff processed the flight-level data. Several folks in HRD helped process the radar data: Mike Black edited the vertical incidence data, shared insights into vertical velocities in hurricanes and generated two figures of vertical velocity for this paper; Nancy Griffin merged the Doppler and reflectivity tapes for PDD analysis; and Paul Leighton and Joe Griffin modified the PDD interpolation software to deal with some of the idiosyncrasies of the Gilbert Doppler dataset. John Gamache developed the variational software and assisted us in applying it to the interpolated Doppler velocities to synthesize the windfields. Wen-Chau Lee and Susan Stringer of the Atmospheric Technology Division of the National Center for Atmospheric Research provided the software (Grid2PS) that produced several figures from the radar data. Comments on an earlier draft by Mike Black and Chris Samsury led to substantial improvements in the paper. Constructive comments from three anonymous reviewers helped us clarify several points in the final version.

APPENDIX

Simple Pressure Retrieval from Pseudo–Dual Doppler Windfields

To retrieve an estimate of the surface pressure from the three-dimensional wind analysis, we calculate pressure perturbations at each level of the axisymmetric mean wind field with a method similar to that in Roux and Viltard (1995). The axisymmetric, nonhydrostatic numerical model of Willoughby et al. (1984) includes an equation [their Eq. (1.1)] for the radial variation of π, the anomaly of the Exner pressure function, ($\Pi = (p/1000)^{R/c_p}$), that was modified to

$$c_p\theta_v\frac{\partial\pi}{\partial r} = -\left[u\frac{\partial u}{\partial r} + w\frac{\partial u}{\partial z} - (v^2 + fv)\right], \quad \text{(A1)}$$

by assuming a steady state and ignoring the diffusion term. The specific heat of dry air is c_p; θ_v is the environmental virtual potential temperature; u and v are the radial and tangential wind, respectively; w is the vertical velocity; f is the Coriolis parameter; and r and z are the radial and vertical distances, respectively. The total perturbation of the Exner function, $\Delta\pi$, for each level is obtained by integrating from the edge of the axisymmetric mean to the center:

$$\Delta\pi = \frac{1}{c_p\theta_v}\int -\left[u\frac{\partial u}{\partial r} + w\frac{\partial u}{\partial z} - (v^2 + fv)\right]dr. \quad \text{(A2)}$$

To recover the pressure perturbation from the Exner function perturbation, use

$$\Delta P = c_p\theta_v\rho\Delta\pi \quad \text{(A3)}$$

(Roux and Viltard 1995). The pressure drop at the level nearest the surface is then applied to a surface pressure estimate at the edge of the domain to estimate the pressure at the center. The environmental virtual potential temperature and density (ρ) at each level are from Sheets's (1969) sounding for the mean environment near tropical cyclones.

REFERENCES

Austin, P. M., and A. C. Bemis, 1950: A quantitative study of the ''bright band'' in radar precipitation echoes. *J. Meteor.,* **7,** 145–151.

Barnes, G., and M. Powell, 1995: The evolution of the inflow boundary layer to Hurricane Gilbert (1988). *Mon. Wea. Rev.,* **123,** 2348–2368.

Black, M. L., and H. E. Willoughby, 1992: The concentric eyewall cycle of Hurricane Gilbert. *Mon. Wea. Rev.,* **120,** 947–957.

——, R. W. Burpee, and F. D. Marks Jr., 1995: Vertical motion asymmetries in the hurricane eyewall. Preprints, *27th Conf. on Radar Meteorology,* Vail, CO, Amer. Meteor. Soc., 574–576.

——, ——, and ——, 1996: Vertical motion characteristics of tropical cyclones determined with airborne Doppler radial velocities. *J. Atmos. Sci.,* **53,** 1887–1909.

Black, R. A., and J. Hallett, 1986: Observations of the distribution of ice in hurricanes. *J. Atmos. Sci.,* **43,** 802–822.

——, H. B. Bluestein, and M. L. Black, 1994: Unusually strong vertical motions in a Caribbean hurricane. *Mon. Wea. Rev.,* **122,** 2722–2739.

Dodge, P., M. Black, R. W. Burpee, and F. D. Marks Jr., 1987: Time-lapse radar imagery from landfalling hurricanes. Preprints, *17th Conf. on Hurricanes and Tropical Meteorology*, Miami, FL, Amer. Meteor. Soc., 166–169.

Dunnavan, G. M., and J. W. Diercks, 1980: An analysis of Super Typhoon Tip (October 1979). *Mon. Wea. Rev.,* **108,** 1915–1923.

Franklin, J. L., S. J. Lord, and F. D. Marks Jr., 1988: Dropwindsonde and radar observations of the eye of Hurricane Gloria (1985). *Mon. Wea. Rev.,* **116,** 1237–1244.

——, ——, S. E. Feuer, and F. D. Marks Jr., 1993: The kinematic structure of Hurricane Gloria (1985), determined from nested analyses of dropwindsonde and Doppler radar data. *Mon. Wea. Rev.,* **121,** 2433–2451.

Gamache, J. F., 1997: Evaluation of a fully three-dimensional variational Doppler analysis technique. Preprints, *28th Conf. on Radar Meteorology,* Austin, TX, Amer. Meteor. Soc., 422–423.

——, R. A. Houze Jr., and F. D. Marks Jr., 1993: Dual-aircraft investigation of the inner core of Hurricane Norbert. Part III: Water budget. *J. Atmos. Sci.,* **50,** 3221–3243.

Hawkins, H. F., and S. M. Imbembo, 1976: The structure of a small, intense hurricane—Inez 1966. *Mon. Wea. Rev.,* **104,** 418–442.

Holliday, C. R., and A. H. Thompson, 1979: Climatological characteristics of rapidly intensifying typhoons. *Mon. Wea. Rev.,* **107,** 1022–1034.

Houze, R. A., Jr., and P. V. Hobbs, 1982: Organization and structure of precipitating cloud systems. *Advances in Geophysics*, Vol. 24, Academic Press, 229–315.

Joint Typhoon Warning Center, 1958–85: Annual typhoon reports. [Available from the National Technical Information Service, 5284 Port Royal Road, Springfield, VA 22601.]

Jordan, C. L., 1958: Mean soundings for the West Indies area. *J. Meteor.,* **15,** 91–97.

——, 1961: Marked changes in the characteristics of the eye of intense typhoons between the deepening and filling stages. *J. Meteor.,* **18,** 779–789.

Jorgensen, D. P., 1984a: Mesoscale and convective-scale characteristics of mature hurricanes. Part I: General observations by research aircraft. *J. Atmos. Sci.,* **41,** 1268–1285.

——, 1984b: Mesoscale and convective-scale characteristics of mature hurricanes. Part II: Inner core structure of Hurricane Allen (1980). *J. Atmos. Sci.,* **41,** 1287–1311.

Lawrence, M. B., and J. M. Gross, 1989: Atlantic hurricane season of 1988. *Mon. Wea. Rev.,* **117,** 2248–2259.

Marks, F. D., Jr., 1985: Evolution of the structure of precipitation in Hurricane Allen (1980). *Mon. Wea. Rev.,* **113,** 909–930.

——, 1992: Kinematic structure of the hurricane inner core as revealed by airborne Doppler radar. Preprints, *Fifth Conf. on Mesoscale Processes,* Atlanta, GA, Amer. Meteor. Soc., 127–132.

——, and R. A. Houze Jr., 1987: Inner core structure of Hurricane Alicia from airborne Doppler radar observations. *J. Atmos. Sci.,* **44,** 1296–1317.

——, R. A. Houze Jr., and J. F. Gamache, 1992: Dual-aircraft investigation of the inner core of Hurricane Norbert. Part I: Kinematic structure. *J. Atmos. Sci.,* **49,** 919–942.

——, D. Atlas, and P. T. Willis, 1993: Probability-matched reflectivity-rainfall relations for a hurricane from aircraft observations. *J. Appl. Meteor.,* **32,** 1134–1141.

Merceret, F. J., and H. W. Davis, 1981: The determination of navigational and meteorological variables measured by NOAA/RFC WP3D Aircraft. NOAA Tech. Memo. ERL RFC-7, 21 pp. [Available from the National Technical Information Service, 5284 Port Royal Rd., Springfield, VA 22601.]

Muramatsu, T., 1986: Trochoidal motion of the eye of Typhoon 8019. *J. Meteor. Soc. Japan,* **64,** 259–272.

Neumann, C. J., B. R. Jarvinen, C. J. McAdie, and J. D. Elms, 1993: *Tropical Cyclones of the North Atlantic Ocean, 1871–1992.* Historical Climatology Series, 6-2, National Climatic Data Center, 193 pp.

Parrish, J. R., R. W. Burpee, F. D. Marks Jr., and C. W. Landsea, 1984: Mesoscale and convective-scale characteristics of Hurricane Frederic during landfall. Preprints, *15th Conf. on Hurricanes and Tropical Meteorology,* Miami, FL, Amer. Meteor. Soc., 415–420.

Powell, M. D., 1990: Boundary layer structure and dynamics in outer hurricane rainbands. Part I: Mesoscale rainfall and kinematic structure. *Mon. Wea. Rev.,* **118,** 891–917.

——, P. P. Dodge, and M. L. Black, 1991: The landfall of Hurricane Hugo in the Carolinas: Surface wind distribution. *Wea. Forecasting,* **6,** 379–399.

Roux, F., and N. Viltard, 1995: Structure and evolution of Hurricane Claudette on 7 September 1991 from airborne Doppler observations. Part I: Kinematics. *Mon. Wea. Rev.,* **123,** 2611–2639.

——, and F. D. Marks Jr., 1996: Extended Velocity Track Display (EVTD): An improved processing method for Doppler radar observations of tropical cyclones. *J. Atmos. Oceanic Technol.,* **13,** 875–899.

Samsury, C., and E. J. Zipser, 1995: Secondary wind maxima in Hurricanes: Airflow and relationship to rainbands. *Mon. Wea. Rev.,* **123,** 3502–3517.

Sheets, R. C., 1969: Some mean hurricane soundings. *J. Appl. Meteor.,* **8,** 134–146.

Steiner, M., R. A. Houze Jr., and S. E. Yuter, 1995: Climatological characterization of three-dimensional storm structure from operational radar and rain gauge data. *J. Appl. Meteor.,* **34,** 1978–2007.

Testud, J., P. H. Hildebrand, and W. C. Lee, 1995: A procedure to correct airborne Doppler radar data for navigation errors, using the echo returned from the earth's surface. *J. Atmos. Oceanic Technol.,* **12,** 800–820.

Weatherford, C. L., and W. M. Gray, 1988: Typhoon structure as revealed by aircraft reconnaissance. Part II: Structural variability. *Mon. Wea. Rev.,* **116,** 1044–1056.

Willoughby, H. E., 1988: The dynamics of the tropical cyclone core. *Aust. Meteor. Mag.,* **36,** 183–191.

——, 1990: Temporal changes of the primary circulation in tropical cyclones. *J. Atmos. Sci.,* **47,** 242–264.

——, 1991: Reply. *J. Atmos. Sci.,* **48,** 1209–1212.

——, and M. B. Chelmow, 1982: Objective determination of hurricane tracks from aircraft observations. *Mon. Wea. Rev.,* **110,** 1298–1305.

——, J. Clos, and M. Shoribah, 1982: Concentric eyewalls, secondary wind maxima, and the evolution of the hurricane vortex. *J. Atmos. Sci.,* **39,** 395–411.

——, H. L. Jin, S. J. Lord, and J. Piotrowicz, 1984: Hurricane structure and evolution as simulated by an axisymmetric, nonhydrostatic numerical model. *J. Atmos. Sci.,* **41,** 1169–1186.

——, J. Masters, and C. Landsea, 1989: A record minimum sea level pressure observed in Hurricane Gilbert. *Mon. Wea. Rev.,* **117,** 2824–2828.